Hindawi
Advances in Civil Engineering
Volume 2021, Article ID 1404568, 9 pages
https://doi.org/10.1155/2021/1404568

Research Article

Using Continuum-Discontinuum Element Method to Model the Foliation-Affected Fracturing in Rock Brazilian Test

Qunlei Zhang,[1,2] Zihan Zhi,[1] Chun Feng,[3] Ruixia Li,[1] Jinchao Yue ,[1] and Junyu Cong[4]

[1]*School of Water Conservancy Engineering, Zhengzhou University, Zhengzhou 450001, China*
[2]*School of Civil Engineering and Communication, North China University of Water Resources and Electric Power, Zhengzhou 450045, China*
[3]*Institute of Mechanics, Chinese Academy of Sciences, Beijing 100190, China*
[4]*Gdem Technology, Beijing, Co., Ltd., Beijing 100096, China*

Correspondence should be addressed to Jinchao Yue; yuejc@zzu.edu.cn

Received 28 April 2021; Accepted 26 June 2021; Published 7 July 2021

Academic Editor: Adolfo Preciado

In this study, the continuum-discontinuum element method (CDEM) was used to investigate the tensile fracture mechanism of rock materials. An isotropic rock disk model and models considering different foliation inclinations were established, and three schemes were used to simulate the rock fracturing in Brazilian test. Then, the influences of the rock matrix and foliation strengths on anisotropy rock fracturing were investigated. Furtherly, simulation results were verified, and the rock fracture mechanisms were discussed. The results show that the rock fracturing in Brazilian test can be accurately simulated by CDEM, which is in accordance with the experimental results. For isotropic and horizontal foliation rock, the stress concentration in loading positions causes a local fracture of rock sample, and application of a local strengthening scheme can simulate the integral tension fracture of sample middle. As the foliation angle varies from 15° to 45°, the rock fracturing is affected by the stress concentration and foliation distribution. In splitting simulation, a strengthening scheme should be adopted to overcome this influence. As a result, the rock sample generates the sliding and compression-shear fracture. As the foliation angle changes from 45° to 75°, the foliation, rather than the matrix, dominates the fracture behavior of rock sample. For vertical foliations' rock, as the middle foliation thickness is appropriately broadened, the simulation results are reasonable. In general, the tensile strength of anisotropic rock entirely decreases with an increase of foliation angle, and the effect of foliation strength on the tensile strength rock sample is larger than that of the rock matrix.

1. Introduction

Because the fracture resistance of rock material is weaker under tension than under compression, so the investigation of rock tensile fracturing is important. The Brazilian disk testing method is usually used to obtain the tensile strength of rock material [1–3]. Meanwhile, rock anisotropy such as fissuring, jointing, and foliation are the important factors in studying the situ stress measurements, displacement control in rock, and excavation damage development. Currently, investigating the fracture mechanism of anisotropy rock materials by Brazilian testing has caused more and more attention.

In experimental research of rock with weak structures, the plastic deformation and failure mechanisms of shale are highly dependent on the orientation of the bedding planes [4–7]. By observing the crack initiation and propagation in the rock, the effect of anisotropy on the failure mechanism was studied, and the failure modes were classified into sliding and nonsliding failure [8–10]. In uniaxial and triaxial compressive strength tests, the shear sliding along the weak planes could reduce the strength of anisotropic rock [11, 12]. Due to the complexity of rock failure, the comprehensive observation and data acquisition of rock fracture process are easily achieved by simulation. The fracturing of the rock sample with a hole was simulated by

the boundary element code DIGS, and the influence of a tensile stress gradient on the rock fracture initiation and crack growth was discussed [13]. The dynamic fracturing characteristics of rock and concrete materials were investigated by the finite element method (FEM) [14, 15]. The extended finite element method (XFEM) was used to evaluate the effect of the specimen flat end in dynamic Brazilian tests [16]. In anisotropic rock mass, due to the interaction of intact rock fracture and joint face sliding, the failure mechanism of rock mass has been discussed by certain studies using the discrete element method (DEM) [17, 18]. Based on the nanoscale structure of shale, a model simulating nanoscale rock anisotropy was proposed [19, 20]. The failure characteristics of phyllite specimens under Brazilian tests are investigated by the particle discrete element method, and the influence of rock foliation strength and matrix microstructure was also studied numerically [21]. A modified smooth joint model was proposed to simulate the failure behavior of jointed rock mass, and the roughness effect of the joint face under different normal stresses was discussed [22–25]. The mechanics behavior of foliated rock samples in the Brazilian tests was simulated using Universal Distinct Element Code (UDEC) [26]. In general, the continuum mechanics method is suitable for analyzing the small deformation and damage behavior of materials, and the discrete element method can easily analyze the rock fracturing and motion. A continuum-discontinuum element method (CDEM) combines the advantages of the finite element method and the discrete element method, which has gradually become an effective simulation method to study the failure mechanisms of rock materials [27–33].

In this context, based on CDEM, the force and deformation of a loading plate in the Brazilian test were analyzed by the continuum element method, and the discontinuum element method was used to study the fracturing of rock samples. An isotropic rock disk model and models considering different foliation angles were sequentially established. The splitting simulations of rock samples were conducted by three simulation schemes. Furthermore, the effects of matrix and foliation strengths on rock fracturing were investigated. Finally, simulation results were verified, and the fracturing mechanisms of rock materials were discussed.

2. Simulation Program

2.1. Simulation Method. In this paper, a coupling method of particle-block element based on the continuum-discontinuum element method (CDEM) is used to investigate the tensile fracture mechanism of rock materials. The simulation method is indicated in Figure 1. CDEM adopts a time-stepping, explicit scheme, and the equilibrium equations are as follows:

$$\begin{aligned} [M]\{\ddot{u}\} + [C]\{\dot{u}\} &= \{F\}_{\text{ext}}, \\ \{F\}_{\text{ext}} &= \{F\}_p + \{F\}_t[F_k], \end{aligned} \tag{1}$$

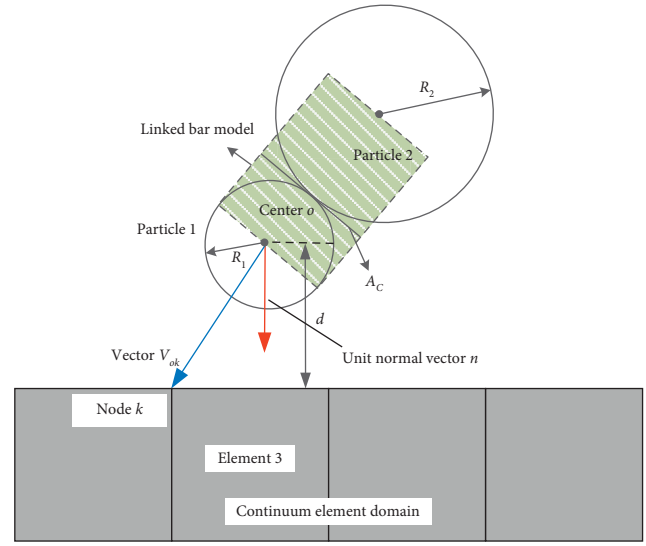

Figure 1: Continuum-discontinuum element model.

where $[M]$ denotes the nodal mass matrix, $[C]$ is the damping matrix, $\{u\}$ denotes the displacement vector, and $\{F\}_{\text{ext}}$ denotes the vector of external forces, which includes the node internal force matrix $[F_k]$, the particle contact force $\{F\}_p$, and external loading force $\{F\}_t$.

For the block elements of the continuum element method, the internal force of the element node in the continuum element method is calculated by

$$[F_k] = \left[F_k^0\right] + \sum_{i=1}^{N} \left[B_i^T\right] \cdot [D] \cdot [B_i] \cdot [\Delta u] \cdot \omega_i \cdot J_i, \tag{2}$$

where $[F_k^0]$ is the node internal force matrix at the previous step, i is the element Gaussian point, N is the number of Gaussian points, $[B_i]$ is the strain matrix, $[\Delta u]$ is the node incremental displacement vector, $[D]$ is the element elastic matrix, ω_i is the integral coefficient, and J_i is the Jacobian determinant value.

For the particle elements of the discontinuum element method, the linked bar model combined with the Mohr–Coulomb criterion and maximum tensile stress criterion is used to simulate the rock breaking and moving [30–32].

The contact forces between two contact particles are calculated by

$$\begin{aligned} F_i(t + \Delta t) &= F_i(t) - K_i \Delta u_i, \quad i = 1, 2, \\ A_c &= \min(2R_i), \quad i = 1, 2, \\ K_i &= \tilde{E}_i A_c (R_1 + R_2), \quad i = 1, 2, \end{aligned} \tag{3}$$

where $F_i(t + \Delta t)$ and $F_i(t)$ are the contact forces at the time of $t + \Delta t$ and t, F_1 and F_2 are the normal and tangential contact forces, Δu_1 and Δu_2 are the normal and tangential increments of contact displacement, R_1 and R_2 represent the radius of contact particles, K_1 and K_2 represent the normal and tangential stiffness, $\tilde{E}_1$ and $\tilde{E}_2$ represent elastic and shear modulus, and A_c is the contact area of particles.

The contact forces of equations (3) are modified by

$$\begin{aligned} &\text{if } F_1 - TA_c \geq 0, \text{ then } F_1 = F_2 = 0, T = C = 0, \\ &\text{if } F_2 - F_1 \tan(\varphi) - CA_c \geq 0, \text{ then } F_2 = F_1 \tan(\varphi), T = C = 0. \end{aligned} \tag{4}$$

In a 2D numerical model, the contact state between block element and particle element is determined by the relative position between particle center and block element boundary. The contact pair will be created when the distance between particle center and block edge is less than or equal to the radius of the particle, that is,

$$d = \left| V_{ok} \cdot n \right| \leq R_1, \tag{5}$$

where d is the distance between particle center and block edge, k is the node of block element, V_{ok} is the relative position vector for particle center o to node k, n is the unit normal vector of continuum element domain boundary, and R_1 is the radius of the particle close to target block element.

2.2. Numerical Models and Parameters. The schematic diagram of Brazilian disk test and isotropic and anisotropic rock models are shown in Figure 2. The rock sample consists of 14154 particles, each with a radius of 0.2 mm. The bearing plate consists of 320 finite element elements. The loading velocity of the top bearing plate is 1 nm/step, and the bottom nodes of the lower bearing plate are fixed. For the anisotropic rock sample, the spacing between foliation planes is 5 mm.

Based on CDEM, the equivalent macrostrain energy of particles with macroscale mechanical parameters coincides well with the strain energy computed by FEM, when the number of contact particles reaches a certain value [32]. The fracturing and moving process of rock is well simulated with macroscale mechanical parameters [31, 32]. The numerical parameters in this study are shown in Table 1 [21].

2.3. Simulation Scheme. To investigate the fracture mechanism of rock materials in Brazilian test, the failure of isotropic rock sample was firstly simulated. Then, the fracturing simulations of rock samples with 0°, 15°, 30°, 45°, 60°, 75°, and 90° foliations were conducted. Finally, the splitting simulations of rock samples with different matrices and foliation strengths were conducted, which were used to investigate the effect of strength parameters on the anisotropic rock failure.

3. Results and Analysis

3.1. Simulation Results of Isotropic Rock and Horizontal Foliation Rock. Adopting different simulation schemes in the Brazilian test, the failure results of isotropic and horizontal foliation rock samples are shown in Figure 3. During the stiff wire loading, the stress concentration near the loading positions causes a local failure of rock sample as shown in model I, and the tensile strength obtained by Brazilian test is smaller than the actual tension strength of rock materials. To solve this problem, a scheme strengthening the local zone of numerical sample is adopted to simulate the splitting of isotropic and horizontal foliation rock. In this scheme, the strengthening zone size is 2 mm × 4 mm, and the local strength parameters are 8 times the strength parameters of Table 1. As shown in model II and III of Figure 3, the integral tensile fracture through the specimen middle can be well simulated. As indicated in the strength histogram, a proper tensile strength of the rock sample in the Brazilian test can be obtained by the splitting simulation, and the tensile strength of isotropic rock sample is slightly larger than that of horizontal foliation rock sample.

3.2. Simulation Results of Rock with Oblique Foliations. For the anisotropic rock with 15°, 30°, 45°, 60°, and 75° foliations, the fracturing processes of rock samples in the Brazilian test were simulated, as shown in Figure 4. To comprehensively analyze the fracture mechanism of anisotropic rock, the strengthening scheme of Section 3.1 was adopted, and simulations without a strengthening scheme were also conducted.

In simulations without a strengthening scheme, as the foliation angle is 15°, the vertical fracture penetrates the entire rock sample, and there only exists a shorter crack propagating along the foliation near the lower loading location of the sample. As the foliation angles are 30° and 45°, two symmetrical cracks generate in two foliations near the upper and lower loading locations. As the foliation angles continue to increase, the orientation of main crack will be closer to the vertical central axis. In simulations with a strengthening scheme, the 15° foliation rock sample fractures along the foliations near the strengthening zone. As the foliation angle is 30°, the strengthening zone covers the foliation near the loading positions, so the cracks propagate along the foliation below the strengthening zone. Meanwhile, the rock sample is crushed in the area between two foliations. As the foliation angles continuously increase from 45° to 75°, the fracture forms of strengthened samples are similar to the fracture forms without a strengthening scheme.

To analyze the effect of foliation angles on the rock tensile strength, the failure strengths of anisotropic rock under two simulation schemes were compared, as shown in Figure 5. For the rock samples with different foliation angles, the failure strengths with a strengthening scheme are entirely larger than those without a strengthening scheme. With a strengthening scheme, the failure strength of rock obviously decreases when the foliation angle changes from 15° to 45°, and then, the failure strength slightly decreases as the foliation angle changes from 45° to 60°. However, the failure strength slightly increases as the foliation angle changes from 60° to 75°. Without a strengthening scheme, the failure strength continuously decreases as the foliation angles increase from 15° to 75°; moreover, the decrease rate of the failure strength of rock with 15° to 30° foliations is obviously larger than that of rock with 30° to 75° foliations.

As indicated in the trend line of Figure 5, studies indicate that the failure strengths of rock with different foliation angles decrease as the foliation angle increases [25, 26]. From Figure 5, as the foliation angle changes from 0° to 45°,

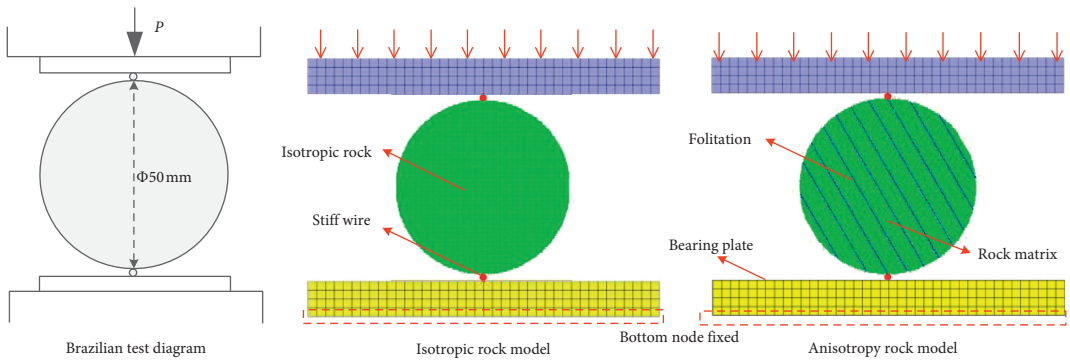

Figure 2: Test diagram and numerical models.

Table 1: Numerical parameters in the simulation of Brazilian test.

	Density (kg/m^3)	Elastic modulus (GPa)	Poisson's ratio	Tensile strength (MPa)	Cohesion (MPa)
Bearing plate	7850	200	0.25	—	—
Rock matrix	2800	30	0.25	6	6
Foliation	2519	24	0.25	2.1	2.16

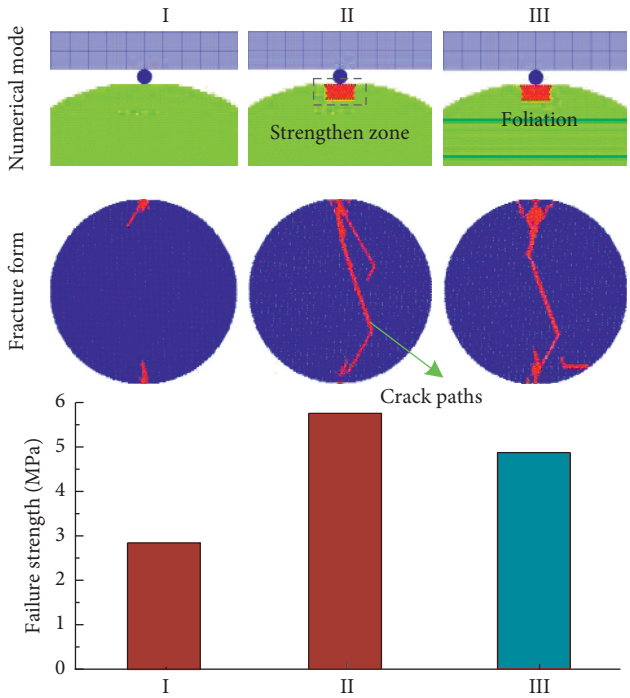

Figure 3: Splitting simulation of isotropic and horizontal foliation rock.

simulation results with a strengthening scheme relatively follow the trend line. However, because the failure strength will continue to decrease as the foliation angle increases from 45° to 75°, simulation results without a strengthening scheme more closely follow the trend line.

3.3. Simulation Results of Rock with Vertical Foliations. Figure 5 of Section 3.2 shows that, as the foliation angle is higher than 75°, the failure strength of the rock sample under a strengthening scheme is obviously higher than the trend line. Therefore, for the splitting of vertical foliation rock, the simulations without a strengthening scheme were conducted, and the effect of foliation thickness in sample middle were also considered, as shown in Figure 6. As the foliation thickness is 0.4 mm, the sample with 90° foliations is crushed near the loading positions, and the main cracks propagate along two foliations near the vertical middle axis of sample. However, as the foliation thickness is 0.8 mm or 1.2 mm, the rock sample is directly split along the middle foliation, and there is only one main crack in the sample. Moreover, the crushing degree near the sample loading positions also decreases. As the foliation thickness increases, the failure strengths of 90° foliation rock obviously decrease, which is consistent with the trend line of Figure 5.

In summary, the effects of different rock foliation angles on the fracture forms and failure strengths of rock samples are significant. For the fracturing simulation of anisotropic rock in the Brazilian test, the splitting process of horizontal foliation rock can be well simulated by a strengthening scheme. The strengthening scheme is also suitable for investigating the fracturing of rock samples with the smaller foliation angle; however, simulations without a strengthening scheme are more suitable for investigating the fracturing of rock samples with the larger foliation angle. Furtherly, the fracturing of the rock sample with vertical foliations can be well simulated by adjusting the foliation thickness of sample middle.

3.4. Simulation Results with Different Rock Matrices and Foliation Strengths. From Figure 5, the failure strength of 45° foliation rock with a strengthening scheme is close to the failure strength without a strengthening scheme. To investigate the effect of foliation and matrix strengths on the rock fracturing, the splitting of 45° foliation rock sample in the Brazilian test was simulated. The tensile and cohesive

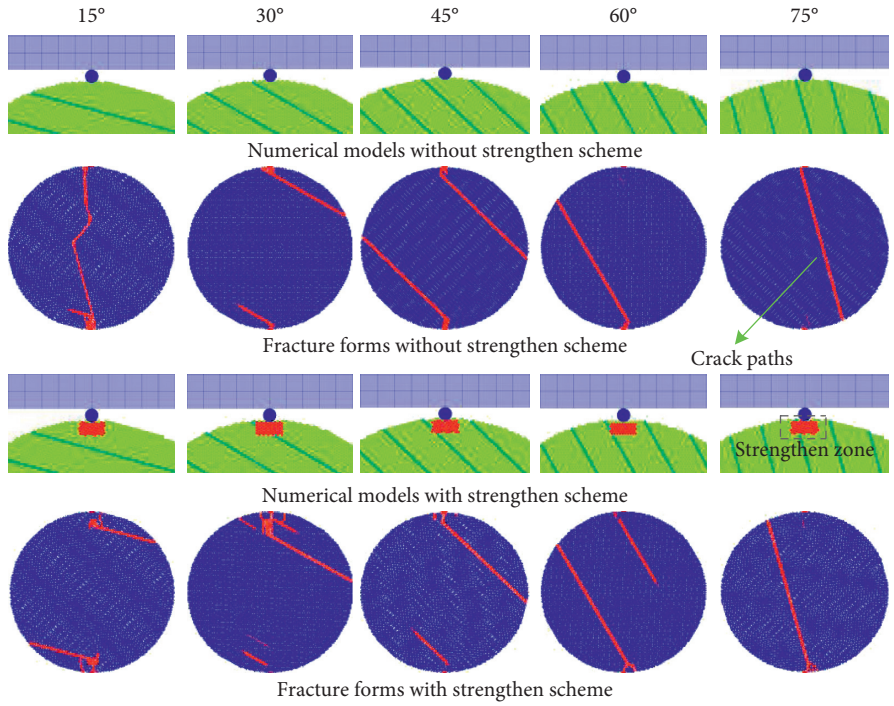

Figure 4: Fracturing simulation of rock with different foliation angles.

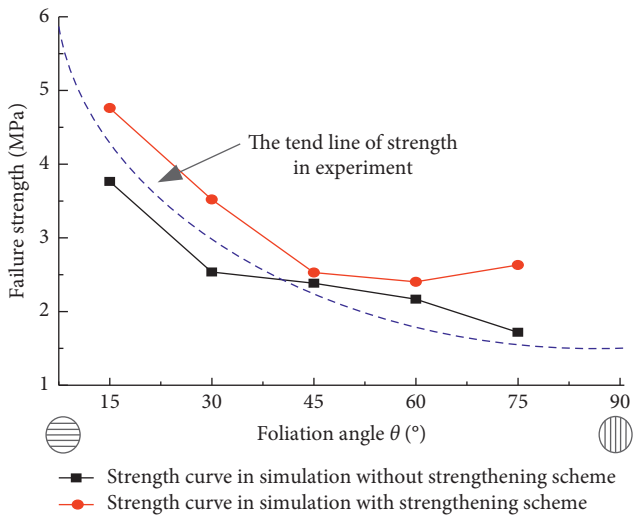

Figure 5: The relationship between foliation angle and failure strength.

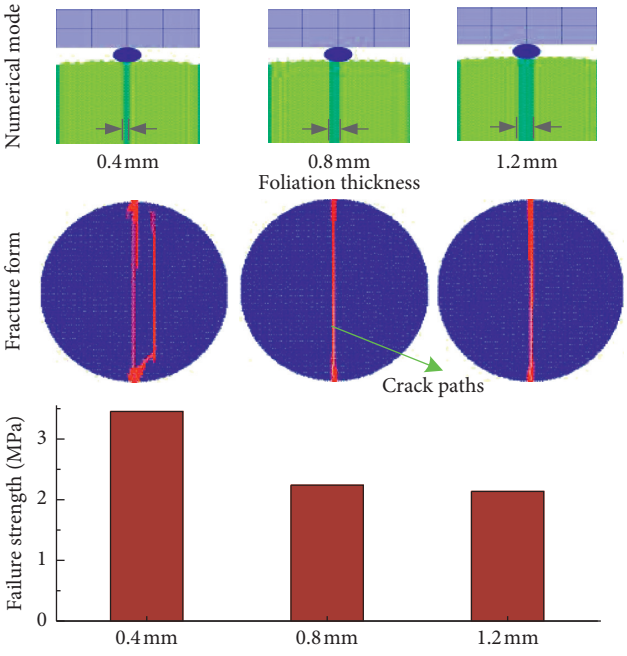

Figure 6: Splitting simulation of vertical foliation rock.

strengths of rock foliation were taken as 1 MPa, 1.5 MPa, 2 MPa, 2.5 MPa, and 3 MPa, respectively. The tensile and cohesive strengths of the rock matrix were taken as 4 MPa, 6 MPa, 8 MPa, 10 MPa, and 12 MPa, respectively.

Under different strength parameters, the tensile failure strengths of the rock sample in the splitting simulation produce significant differences, as shown in Figure 7. As the foliation strengths increase, the failure strengths of the rock sample increase. Specifically, as the foliation tensile strength varies from 1 MPa to 3 MPa, the tensile failure strength of rock sample changes from 2.28 MPa to 2.44 MPa. As the foliation cohesive strength varies from 1 MPa to 3 MPa, the tensile failure strength of the rock sample changes from 2.2 MPa to 2.43 MPa. Moreover, the tensile failure strength of the rock sample also increases with an increase of rock matrix strength. As the matrix tensile strength varies from 4 MPa to 12 MPa, the tensile failure strength of the rock sample increases from 2.1 MPa to 2.9 MPa. As the matrix cohesive strength varies from 4 MPa to 12 MPa, the tensile failure strength of rock sample changes from 2.2 MPa to 2.7 MPa.

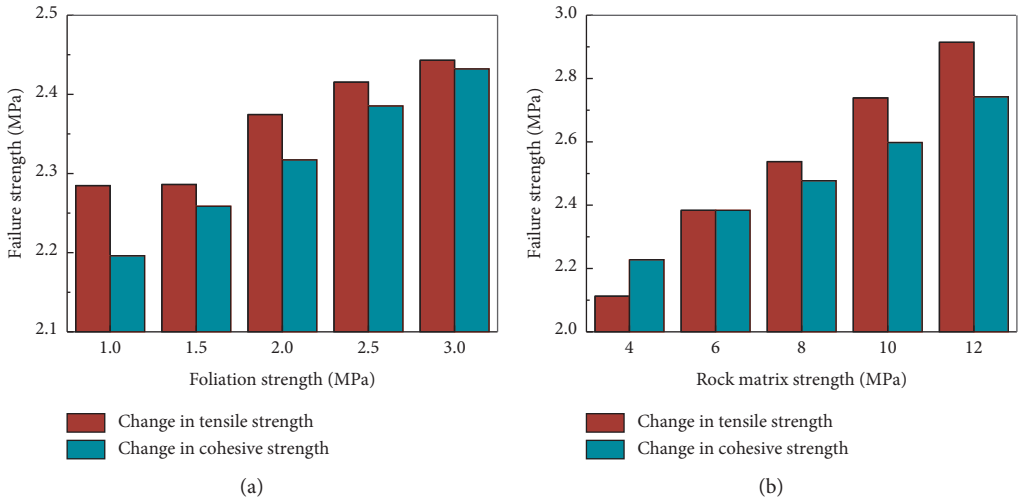

Figure 7: Failure strengths of rock samples with different foliation and matrix strengths.

In general, for the splitting simulations of 45° foliation rock sample, the variation range of rock matrix strengths is 4 MPa to 12 MPa; however, the foliation strengths vary from 1 MPa to 3 MPa. As the results of the splitting simulation, the tensile failure strengths of rock samples only change from 2.1 MPa to 2.9 MPa. This indicates the effect of matrix strength variation on the tensile strength of the rock sample is not obvious; however, the foliation strength variation significantly affects the tensile strength of the rock sample.

4. Verification and Discussion

4.1. Verification. To verify the simulation results, the current works are compared with [25, 26], as shown in Figure 8. In general, the fracture patterns of foliation rock in current simulation are consistent with those of laboratory tests. As the foliation angle is 0°, the rock sample fractures along the vertical middle axis. As the foliation angle increases, the cracks of rock samples mainly propagate along rock foliations. Specifically, as the foliation angle is 0°, the loading positions of the rock sample are crushed in current work, and a corner breakage also occurs near the loading positions of 0° foliation rock in [25]. Meanwhile, there is a short horizontal crack in the lower part of the rock sample in current work, and there is also a crack along the foliation of rock sample in [26].

4.2. Discussion. In this study, the fracturing processes of isotropic and anisotropic rock samples in the Brazilian test were simulated, and simulation results are consistent with the experiment results. The fracture mechanism of the rock sample in the Brazilian test can be well depicted by the continuum-discontinuum element method.

In Brazilian splitting test, the vertical load firstly applies to the rock matrix near the sample loading positions, and then, the vertical load gradually translates into the sample middle. For the isotropic and horizontal foliation rock in the splitting simulation of Brazilian test, the failure tensile strengths of rock samples are larger than those of the inclined and vertical foliation rock, so the isotropic and horizontal foliation rock samples relatively easily generate the compression-shear fracture and the integral tensile fracture. During the stiff wire loading, the stress concentration near the loading positions easily causes the local failure of the rock sample, and the tensile strength obtained by splitting simulation is smaller than the actual tension strength of rock materials. Therefore, for the isotropic and horizontal foliation rock, a local strengthening scheme should be adopted to simulate the splitting of rock samples, which can simulate the integral tensile fracture and obtain the proper tension strength of the rock sample in the Brazilian test. As rock foliation angles vary from 15° to 45°, the tensile strength variation of numerical samples with a strengthening scheme is consistent with the trend of Figure 5, and the rock samples generate the compression-shear fracture and the sliding fracturing along the foliations. This indicates as the foliation angle is smaller, the stress concentration and rock foliation both affect the splitting results of the rock sample. As rock foliation angles varies from 45° to 75°, the rock samples only generate the fracturing along the foliations; moreover, the tensile strength variation in simulation with a strengthening scheme is obviously different from the trend of Figure 5. This indicates the effect of larger angle foliations on sample splitting is larger than the rock matrix. The fracturing of vertical foliation rock can be well simulated by adjusting the foliation thickness of sample middle, which can be because, in the complex geological processes, the geometric widthess of rock foliation appears to be very small; however, the influence area of the weak layer structure on the rock sample may be much larger than that of its geometric size.

With the strength parameter variation of the rock foliation and matrix, the weak layer structures have a significant influence on the fracture form and failure strength of anisotropic rock, although rock matrix strengths are much higher than foliation strengths. Therefore, the adjustment of rock matrix strength cannot obviously change the tensile failure strength of the numerical sample, while the

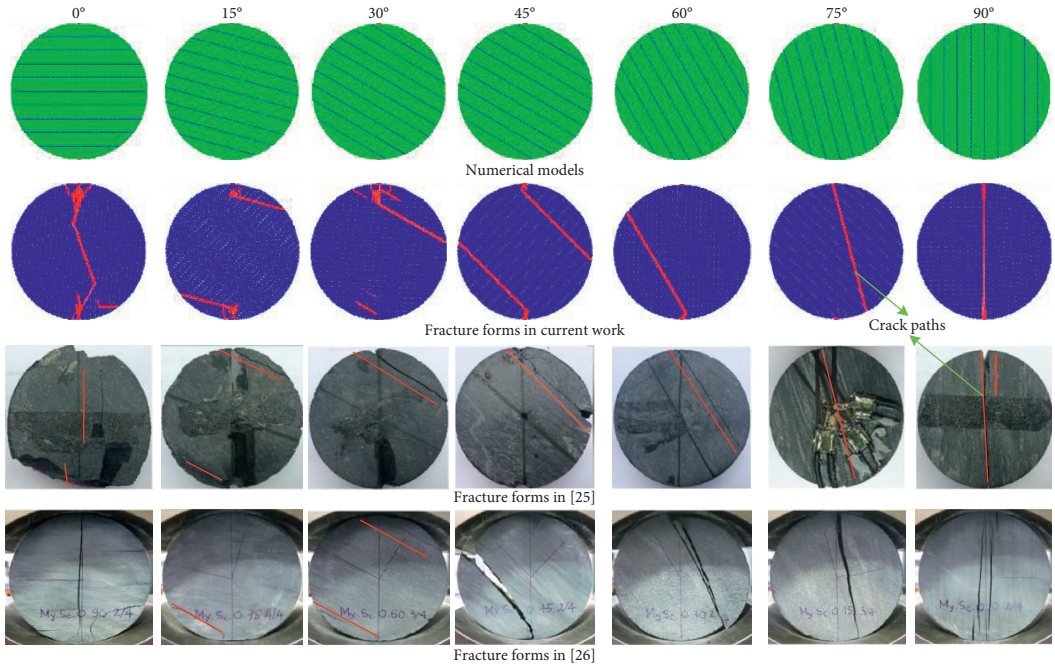

Figure 8: Comparison of simulation and experiment.

variation in the foliation strength can significantly affect the tensile failure strength of the rock sample.

5. Conclusions

(1) The fracturing of rock samples in the Brazilian test can be well simulated by the continuum-discontinuum element method (CDEM), and simulation results are consistent with the literatures. For isotropic and horizontal foliation rock samples, the stress concentration easily causes the local failure of the sample, and the effect of the rock matrix on splitting of numerical samples is larger than rock foliation. The splitting of the rock sample can be simulated by a strengthening scheme. Isotropic and horizontal foliation rock easily generates the compression-shear fracture near loading positions and integral tensile fracture in sample middle.

(2) As foliation angle varies from 15° to 45°, the foliations and the stress concentration near loading positions both affect the splitting results of the rock sample. Rock samples easily generate the sliding fracturing along foliations and the compression-shear fracturing near loading positions. As foliation angles varies from 45° to 75°, the tensile strength variation of the rock sample without a strengthening scheme is consistent with experiment results, the effect of rock foliation on sample splitting is larger than the rock matrix, and the rock samples mainly generate the fracturing along foliations. The fracturing of vertical foliation rock can be well simulated by adjusting the foliation thickness of sample middle, and the influence area of the foliation on the rock sample may be larger than that of its geometric size.

(3) For the fracturing of the rock sample with 45° foliations, as the tensile strength of foliation varies from 1 MPa to 3 MPa, the rock failure strength increases from 2.28 MPa to 2.44 MPa. The rock failure strength changes from 2.2 MPa to 2.43 MPa as the cohesive strength of foliation varies from 1 MPa to 3 MPa. However, as the tensile strength of the rock matrix varies from 4 MPa to 12 MPa, the rock failure strength changes from 2.1 MPa to 2.9 MPa. The rock failure strength changes from 2.2 MPa to 2.7 MPa as the cohesive strength of rock matrix changes from 4 MPa to 12 MPa. This indicates the rock foliation rather than the rock matrix dominates the failure strength of the rock sample.

Data Availability

The data used to support the findings of this study are included within the article.

Conflicts of Interest

The authors declare that they have no conflicts of interest to report regarding the present study.

Acknowledgments

This work was supported by the National Key R&D Program of China (Grant nos. 2018YFC0604502 and 2018YFC1505504) National Natural Science Foundation of China (Grant no. 51708513), China Postdoctoral Science Foundation (Grant no. 2020M672227), and Henan

Provincial Department of Transportation (Grant nos. 2018J4 and 2019J1). The authors gratefully acknowledge Dr. Shen Wang and Professor Ruifu Yuan in Henan Polytechnic University, who provided language help and writing assistance.

References

[1] C.-S. Chen, E. Pan, and B. Amadei, "Determination of deformability and tensile strength of anisotropic rock using Brazilian tests," *International Journal of Rock Mechanics and Mining Sciences*, vol. 35, no. 1, pp. 43–61, 1998.

[2] Q. Z. Wang, W. Li, and H. P. Xie, "Dynamic split tensile test of flattened Brazilian disc of rock with SHPB setup," *Mechanics of Materials*, vol. 41, no. 3, pp. 252–260, 2009.

[3] K. H. Li, Y. M. Cheng, and X. Fan, "Roles of model size and particle size distribution on macro-mechanical properties of Lac du Bonnet granite using flat-joint model," *Computers and Geotechnics*, vol. 103, pp. 43–60, 2018.

[4] G. Barla and L. Goffi, "Direct tensile testing of anisotropic rocks," in *Proceedings of the 3rd Congress of the International Society for Rock Mechanics*, Denver, CO, USA, 1974.

[5] H. Niandou, J. F. Shao, J. P. Henry, and D. Fourmaintraux, "Laboratory investigation of the mechanical behaviour of Tournemire shale," *International Journal of Rock Mechanics and Mining Sciences*, vol. 34, no. 1, pp. 3–16, 1997.

[6] J.-W. Cho, H. Kim, S. Jeon, and K.-B. Min, "Deformation and strength anisotropy of Asan gneiss, Boryeong shale, and Yeoncheon schist," *International Journal of Rock Mechanics and Mining Sciences*, vol. 50, pp. 158–169, 2012.

[7] B. Debecker and A. Vervoort, "Experimental observation of fracture patterns in layered slate," *International Journal of Fracture*, vol. 159, no. 1, pp. 51–62, 2009.

[8] T. Meier, E. Rybacki, T. Backers, and G. Dresen, "Influence of bedding angle on borehole stability: a laboratory investigation of transverse isotropic oil shale," *Rock Mechanics and Rock Engineering*, vol. 48, no. 4, pp. 1535–1546, 2015.

[9] A. Tavallali and A. Vervoort, "Effect of layer orientation on the failure of layered sandstone under Brazilian test conditions," *International Journal of Rock Mechanics and Mining Sciences*, vol. 47, no. 2, pp. 313–322, 2010.

[10] B. Debecker and A. Vervoort, "Two-dimensional discrete element simulations of the fracture behaviour of slate," *International Journal of Rock Mechanics and Mining Sciences*, vol. 61, pp. 161–170, 2013.

[11] B. Park and K.-B. Min, "Bonded-particle discrete element modeling of mechanical behavior of transversely isotropic rock," *International Journal of Rock Mechanics and Mining Sciences*, vol. 76, pp. 243–255, 2015.

[12] U. Kuila, D. N. Dewhurst, A. F. Siggins, and M. D. Raven, "Stress anisotropy and velocity anisotropy in low porosity shale," *Tectonophysics*, vol. 503, no. 1, pp. 34–44, 2011.

[13] B. V. D. Steen, A. Vervoort, and J. A. L. Napier, "Observed and simulated fracture pattern in diametrically loaded discs of rock material," *International Journal of Fracture*, vol. 131, no. 1, pp. 35–52, 2005.

[14] S. H. Cho, Y. Ogata, and K. Kaneko, "Strain-rate dependency of the dynamic tensile strength of rock," *International Journal of Rock Mechanics and Mining Sciences*, vol. 40, no. 5, pp. 763–777, 2003.

[15] Y. Hao and H. Hao, "Finite element modelling of mesoscale concrete material in dynamic splitting test," *Advances in Structural Engineering*, vol. 19, no. 6, pp. 1027–1039, 2016.

[16] M. R. Khosravani, M. Silani, and K. Weinberg, "Fracture studies of ultra-high performance concrete using dynamic Brazilian tests," *Theoretical and Applied Fracture Mechanics*, vol. 93, pp. 302–310, 2018.

[17] D. O. Potyondy and P. A. Cundall, "A bonded-particle model for rock," *International Journal of Rock Mechanics and Mining Sciences*, vol. 41, no. 8, pp. 1329–1364, 2004.

[18] N. Cho, C. D. Martin, and D. C. Sego, "A clumped particle model for rock," *International Journal of Rock Mechanics and Mining Sciences*, vol. 44, no. 7, pp. 997–1010, 2007.

[19] B. E. Hornby, L. M. Schwartz, and J. A. Hudson, "Anisotropic effective-medium modeling of the elastic properties of shales," *Geophysics*, vol. 59, no. 10, pp. 1570–1583, 1994.

[20] R. N. Vasin, H. R. Wenk, W. Kanitpanyacharoen, S. Matthies, and R. Wirth, "Elastic anisotropy modeling of Kimmeridge shale," *Journal of Geophysical Research: Solid Earth*, vol. 118, no. 8, pp. 3931–3956, 2013.

[21] G. Xu, C. He, Z. Chen, and A. Su, "Transverse isotropy of phyllite under Brazilian tests: laboratory testing and numerical simulations," *Rock Mechanics and Rock Engineering*, vol. 51, no. 4, pp. 1111–1135, 2018.

[22] C.-C. Chiu, T.-T. Wang, M.-C. Weng, and T.-H. Huang, "Modeling the anisotropic behavior of jointed rock mass using a modified smooth-joint model," *International Journal of Rock Mechanics and Mining Sciences*, vol. 62, pp. 14–22, 2013.

[23] X.-X. Yang, H.-W. Jing, C.-A. Tang, and S.-Q. Yang, "Effect of parallel joint interaction on mechanical behavior of jointed rock mass models," *International Journal of Rock Mechanics and Mining Sciences*, vol. 92, pp. 40–53, 2017.

[24] X.-X. Yang, H.-W. Jing, and W.-G. Qiao, "Numerical investigation of the failure mechanism of transversely isotropic rocks with a particle flow modeling method," *Processes*, vol. 6, no. 9, p. 171, 2018.

[25] G. Xu, C. He, Z. Chen, and D. Wu, "Effects of the microstructure and micro-parameters on the mechanical behaviour of transversely isotropic rock in Brazilian tests," *Acta Geotechnica*, vol. 13, no. 4, pp. 887–910, 2018.

[26] X. Tan, H. Konietzky, T. Frühwirt, and D. Q. Dan, "Brazilian tests on transversely isotropic rocks: laboratory testing and numerical simulations," *Rock Mechanics and Rock Engineering*, vol. 48, no. 4, pp. 1341–1351, 2015.

[27] L. Wang, S. Li, G. Zhang, Z. Ma, and L. Zhang, "A GPU-based parallel procedure for nonlinear analysis of complex structures using a coupled FEM/DEM approach," *Mathematical Problems in Engineering*, vol. 2013, Article ID 618980, 15 pages, 2013.

[28] Q. L. Zhang, Z. H. Zhi, C. Feng, Y. C. Cai, G. H. Pang, and J. C. Yue, "Investigation of concrete pavement cracking under multi-head impact loading via the continuum-discontinuum element method," *International Journal of Impact Engineering*, vol. 135, Article ID 103410, 2020.

[29] Z. Chen, W. Gong, G. Ma et al., "Comparisons between centrifuge and numerical modeling results for slope toppling failure," *Science China Technological Sciences*, vol. 58, no. 9, pp. 1497–1508, 2015.

[30] Q. L. Zhang, R. F. Yuan, S. Wang, D. Y. Li, H. M. Li, and X. H. Zhang, "Optimizing simulation and analysis of automated top-coal drawing technique in extra-thick coal seams," *Energies*, vol. 13, no. 1, 2020.

[31] Q. L. Zhang, J. C. Yue, C. Liu, C. Feng, and H. M. Li, "Study of automated top-coal caving in extra-thick coal seams using the continuum-discontinuum element method," *International*

Journal of Rock Mechanics and Mining Sciences, vol. 122, Article ID 104033, 2019.

[32] C. Feng, S. H. Li, and X. Y. Liu, "Particle-dem based linked bar strain softening model and its application," *Chinese Journal of Theoretical and Applied Mechanics*, vol. 48, pp. 76–85, 2016.

[33] R. Yuan and B. Shen, "Numerical modelling of the contact condition of a Brazilian disk test and its influence on the tensile strength of rock," *International Journal of Rock Mechanics and Mining Sciences*, vol. 93, pp. 54–65, 2017.